to be published in: ***Journal of Material Science: Materials in Electronics***

Coherent defect spectroscopy with pulsed optically and electrically detected magnetic resonance

C. Boehme[1], K. Lips[2]

[1]University of Utah, Department of Physics,
115 S 1400 E Suite 201, Salt Lake City, Utah 84112-0830, USA

[2]Hahn-Meitner-Institut Berlin, Kekuléstraße 5, D-12489 Berlin, Germany

A short review of the theoretical and experimental foundations of pulsed optically and electrically detected magnetic resonance (pODMR and pEDMR, respectively) as well as their fields of applications is given. In comparison to electron spin resonance spectroscopy, ODMR and EDMR can be 8-10 orders of magnitude more sensitive which make them particularly useful for the investigation of defects in low dimensional material systems and thin-film devices. In recent years, there has been quite a significant progress with pODMR and pEDMR which provide quantitative access to spin-coherence times, coupling constants and inhomogeneities of the investigated defect systems.

Corresponding author email: boehme@physics.utah.edu

to be published in: ***Journal of Material Science: Materials in Electronics***

1. Introduction

Optically and electrically detected magnetic resonance (ODMR and EDMR, respectively) are spin spectroscopy methods where the spin measurement is conducted indirectly through detection of spin-dependent electronic transitions by means of their photoluminescence (PL) or with current measurements. ODMR and EDMR have been used extensively for more than 40 years [1,2] as continuous-wave (cw) methods for the microscopic investigation of the properties and the electronic activity (transport, recombination) of a wide range of defects in many semiconductor systems and even in devices under operating conditions [3,4]. Continuous wave means the measurement is carried out as magnetic field-sweep experiment under continuous exposure of the sample to microwave radiation. The magnetic resonances are then detected by sample PL or conductivity changes at distinct magnetic fields from which Landé factors of the corresponding paramagnetic centres are derived. In comparison to electron spin resonance spectroscopy (ESR), ODMR and EDMR are up to 8-10 orders of magnitude more sensitive and both have proven to attain single spin sensitivity [5,6], which makes them particularly useful for the investigation of low dimensional material systems and devices. The limitations of cw ODMR/EDMR lie in the difficult quantitative access to any other information than the Landé factors. Spin-coherence times, the transition times of the spin-dependent recombination and transport mechanisms involved or coupling constants can not be extracted from cw EDMR/ODMR experiments due to their complicated convolution into the shape and the width of cw EDMR/ODMR line shapes. Because of these limitations, coherent, pulsed (p)ODMR and pEDMR have been developed for semiconductors [7-9]. The sensitive observation of coherent spin motion provided by these experiments allows utilizing many advantages known from pulse ESR [10] or pulsed nuclear magnetic resonance techniques. The transient observation of the spin propagation provides an extended set of experimental parameters such as pulse intensities, length, phases etc. and, due to the applicability of various pulse sequences, a much greater set of observables becomes accessible.

In the following, an overview about the state of the development of pEDMR and pODMR as used for the investigation of defects involved in spin-dependent transitions in semiconductors is presented. The general nature of the microscopic processes which are used for these methods is discussed, the principles behind the electrical or optical observation of spin-Rabi oscillation are introduced and, for the example of optically detected recombination in hydrogenated amorphous

silicon (a-Si:H), experimental data is presented and conclusions and interpretations from the data are given.

2. Spin selection rules and spin-dependent transitions

Basis of any electrical or optical spin measurement is always a mechanism which allows a spin state to control electronic transitions which then influence the PL or the conductivity of a material. There are two principally different classes of spin-dependent transitions: The first class consists of energetically resonant transitions where the spin dependency results from the different energy levels of different spin states. The electron with a spin state whose energy level is closer to the state into which a transition is to be taking place will have a higher transition probability. Note that this kind of spin-dependent processes is what determines most spintronics applications. The spin dependency becomes more pronounced with increasing energy splitting which is why the observable effects due to these transitions are most pronounced in materials with large or gigantic Zeeman effects [11]. Many III-V semiconductor materials fall into this category because of their strong spin-orbit coupling. Magnetic resonance experiments and therefore EDMR are difficult to perform with these systems because of the large Zeeman splitting and the entanglement of the spin states with electronic states. To perform ODMR experiments is even more difficult in these materials since no radiation is emitted when the energy is conserved as it is the case for resonant electronic transitions. The second class of spin-dependent transitions are those between paramagnetic states that are governed by spin-selection rules. As electrons undergo transitions into singly occupied states, a double occupied electron-pair state is formed whose spin-pair state must be a singlet because of Pauli's exclusion principle. When spin conservation is given, as it is the case for materials with weak spin-orbit coupling, a transition from two paramagnetic one-electron states into a diamagnetic two-electron state is only allowed when the spin-pair state of two electrons has singlet content before the transition takes place. It is stressed that this second class of spin-dependent mechanisms occurs only in weakly spin-orbital coupled systems. Thus, it represents exactly the opposite coupling situation as the first class of spin-dependent mechanisms in strongly spin-orbital coupled systems. Examples for such mechanisms are typically found in group IV semiconductors as well as organic semiconductors [3,12,13].

Figure 1 illustrates spin-dependent transitions due to spin-selection rules which can be detected with EDMR and ODMR. Case (a) describes spin-dependent transport. The model illustrated is described in detail in Ref. [8]. It consists of hopping or tunnelling transport through two sets of different but spatially adjacent defect sites referred to as sites A and B, respectively. There is an energy match or a near energy match between the singly occupied state of one site and the doubly occupied state of the other site. Such A-B pair sites can be found in many disordered semiconductors at low temperature where electronic transport takes place mostly by hopping transitions through localized bandtail states. Due to the wide distribution of the bandtail state energies and their high densities, there will always be a number of A-B pair sites which contribute a measurable spin-dependent current [14]. Figure 1(b) illustrates spin-dependent recombination for the example of recombination through localized donor (D) and acceptor (A) states. Beside D-A recombination [15], spin-dependent recombination has been observed in a variety of qualitatively different mechanisms such as weakly bound excitonic states and tail-tail recombination [7,16] (the experimental data reviewed in sections 4 and 5 will be concerned with these examples), bandtail-deep defect recombination [17] or direct capture recombination at deep defects [18]. Even though all these mechanisms are of quite different microscopic nature, they can all be spin dependent as long they involve electronic transitions between two paramagnetic states. Historically, this realization that all these different systems are unified by pairing of two paramagnetic electronic states (also referred to as intermediate electron pair-state), was made by Kaplan et al. [19] in 1978, after several unsuccessful attempts to explain the temperature and magnetic-field dependencies of EDMR signal amplitudes. A summery of this quest to find a correct model for spin-dependent recombination can be found in chapter 2 of Ref. [20].

3. pEDMR/pODMR experiments on semiconductors

There are several challenges that pODMR but most of all pEDMR pose in comparison to pESR experiments. For pESR, real-time transients of the radiation emitted by the investigated spins are detected after a coherent spin excitation. In contrast, for pODMR and pEDMR it is in most cases impossible to conduct a real-time observation of transport or recombination transients. This applies in particular to the electrical detection. Any rate change will leave its imprint on a measured sample current with a delay determined by the dielectric relaxation time of the host material. The dielectric relaxation time is the product of the sample resistivity and the dielectric constant. Obviously, for semiconductors at low temperature, this product can become high

enough to deteriorate the time resolution of a transient current measurement beyond the time range on which coherent spin propagation takes place. Another challenge for pEDMR is the presence of large microwave-induced spin-independent artefact currents. Since subtle currents are measured while very intensive microwave pulses are applied to the sample, a large base signal due to the simple absorption of radiation (antenna effect) is induced. Due to their independence of the externally applied magnetic field (as long as magnetoresistance effects do not play a role), these currents are distinguishable from the subtle spin-dependent signals and, therefore, subtractable as constant background. However, they induce shot noise which typically limits the signal to noise ratio of the experiments. In contrast to electrical detection, optically detected PL always reflects transitions that determine light emissions such as radiative or a competing non-radiative channels. Thus, for pODMR, both, the delay problem as well as the microwave artefact problem are not existent or not as critical as compared to pEDMR. This is probably why the first pODMR experiments preceded first pEDMR experiments by more than two decades [21,22]. However, applied to narrow band gap semiconductors (such as crystalline silicon), the emitted infrared radiation with long wavelength may also limit the detectable time resolution beyond the time scale of the coherent spin motion, especially when only smallest PL changes are detected on top of a large PL intensity.

In order to overcome the constraints of the limited time resolution given by the light or current detection, many pODMR and all pEDMR experiments on semiconductors are conducted in the way illustrated in Fig. 2 on a logarithmic time scale. Before the experiment, the system is brought into a non-equilibrium steady state, where the continuous generation of charge carriers leads to a constant recombination rate. While the four eigenstates of the two-spin s=1/2 pairs are generated with equal probability when spin polarization is negligible (this is the case at typical X-band ESR magnetic fields and liquid ^{4}He temperature), the approach to the steady state will pump triplet states to very high densities because of their much longer lifetimes in comparison to eigenstates with singlet content. Hence, once the spin-pair ensemble is initialized into triplet states (note that these are paramagnetic states), it can be manipulated with magnetic resonance. A coherent manipulation requires an exciting pulse short enough such that spontaneous spin or electronic transitions are negligible during the duration of the pulse. After the pulse, the pair will generally not be in an eigenstate anymore, it will be in a coherent superposition $|\Psi\rangle$ of eigenstates that have non-vanishing singlet content. The singlet content of $|\Psi\rangle$ depends on the pulse parameters such as excitation length, intensity, and frequency. After the transition rate is

changed by the microwave pulse, it will retain its value and, only gradually, it will relax back to the steady state on a time scale orders of a magnitude longer than the pulse length. The mechanisms behind this relaxation are incoherent processes such as spin relaxation, transport or recombination transitions (the latter two make the entire process detectable), and spontaneous spin-pair dissociation. Note that the integral Q of the rate transient represents the overall number of transitions that take place due to the pulse excitation [8,23]. For pODMR, Q represents a number of photons whereas for pEDMR, it represents the charge that recombines or passes through a sample due to the application of the ESR pulse. It is the observable Q which represents the actual coherent measurement of the spin-pair state at the end of the pulse. Since $Q \propto |\langle S|\Psi\rangle|^2$ [8, 23, 24], Q is a measure for the singlet content of the pair, or in order words, pEDMR and pODMR are measurement methods for spin-pair permutation symmetries.

4. An experimental example: pODMR on a-Si:H

In the following, pODMR on nominally intrinsic a-Si:H is reviewed as an example that shows how the spin propagation during a coherent excitation can be observed and what insights can be gained from such measurements. All experiments presented in the following were performed on i-a-Si:H, deposited on 1737 Corning glass by plasma-enhanced chemical vapor deposition as described in detail in Ref. [25]. The sample was light soaked before the experiments. The experiments were performed at a temperature of T = 10K. The PL was stimulated by excitation with the 514nm Ar+ ion laser line which yielded a generation rate of $10^{22}cm^{-3}s^{-1}$. The PL was collected by a fiber bundle and detected as a spectrally integrated signal by an InGaAs detector. For the given measurement conditions and the detected PL, fastest coherence times in the upper ns to lower μs range were supposed to be expected. Thus, the coherent spin propagation during the pulse excitation had to take place in a time range of a few hundred ns corresponding to electron spin Rabi oscillation frequencies above 10MHz. Because of this, a microwave field-strength, B_1, of about 1mT was necessary (equivalent to 1kW power).

4.1. Relaxation of a coherent excitation

Figure 3 displays the transient response of the PL after a short coherent microwave pulse for different applied magnetic fields. The plot displays a 6mT wide structure centred at $B_0 \approx$ 345mT ($g \approx 2.009$). The ESR pulse induces an increase of the PL intensity which relaxes back to its

steady state within approximately 5μs. Also, in the colour plot with linear scaling hardly recognizable (violet on blue) a very slowly relaxing quenching signal appears at about $B_0 \approx$ 346mT ($g \approx 2.005$) in agreement with previous cw ODMR measurements on i-a-Si:H [26]. In contrast to these cw ODMR spectra, the two dimensional measurement of the PL as a function of the magnetic field and the time allows to distinguish the magnetic resonance induced effects on the fast relaxing strong enhancement signal and the slowly relaxing weak quenching signal. Clearly, since the pulsed excitation enhances singlet densities as explained above, the strong enhanced PL is indicative (yet not a proof) for a radiative recombination channel whereas the weak quenching channels around the Landé factors of the dangling bond ($g \approx 2.005$) is indicative for a competing non-radiative channel which quenches the detected radiative channels.

4.2. Optically detected spin-Rabi oscillation and spin-echo effects

As pointed out in chapter 3, an integration of the pODMR transient reflects the singlet content of the exited spin-pair state at the end of the microwave pulse. Hence, a measurement of the integral Q as a function of the pulse length reveals the propagation of the singlet content while the pulse is applied. Note that when the coupling between the two spins in a given pair is weak (exchange (J) and dipolar coupling strength (D) are smaller than the separation between the Larmor frequencies ($\Delta\omega$) of the spins [24]) and the microwave field is not too strong either ($B_1 < \Delta\omega$ [24]), only one of the two spin pairs is in resonance and the singlet density oscillates with the frequency of the Rabi nutation of the spin in resonance. Hence, the observed oscillation of the PL during the excitation reflects the Rabi oscillation of the excited spin which precesses with a frequency $\Omega = \gamma B_1$. This is the nutation frequency of a particle with spin $s = 1/2$. Here, $\gamma = g\mu_B/\hbar$ is the gyromagnetic ratio. When the coupling between the spins exceeds $\Delta\omega$ [24, 27], both spins will be excited at the same time. Evidently, the identical spin motion of the two $s = 1/2$ spins will cause the permutation symmetry to oscillate with a frequency $\Omega = 2\gamma B_1$. This is just twice the nutation frequency of an $s = 1/2$ spin [23, 24]. Hence, the detection of the frequency components of pODMR signal during the excitation allows the distinction of different coupling regimes of different pairs even when the decay dynamics are identical.

Figure 4 displays the measurement of Q as a function of the pulse length, τ, under otherwise identical conditions as for the data presented in fig. 3. Note that Q was obtained from an integration of the PL intensity over the time interval indicated by the bar in fig. 3. This

integration interval was chosen such that both the strong, quickly decaying signal and the weak, slowly decaying signal around $g = 2.005$ were taken into account. During the interval between $\tau = 0$ and $\tau = 200$ns, one can clearly recognize an oscillatory behaviour of the transient whereas with several frequency components. The oscillation intensity drops off within a few cycles. This fast drop-off reduces the interpretability of the data since a Fourier transform will reveal broad frequency peaks which may reduce the resolvability of the different components. An improvement can be achieved with an optically detected rotary echo which is carried out by means of a 180^o phase change of the exciting microwave field which is introduced at a moment when most of the oscillation has decayed (here, the moment was chosen to be $\tau = \tau_{180} = 200$ns). When the decay of the initial oscillation is not due to incoherence induced by very fast recombination processes but instead, it is due to coherent dephasing of the spin ensemble due to an inhomogeneity of the spin's Rabi frequencies [23], the spin ensemble will partially regain its phase after the phase jump and the oscillation will become visible again at $\tau = 2\tau_{180}$ (= 400ns here) before it again dephases. This temporary rephrasing is called echo, the details and the nature of this effect with regard to spin-dependent recombination are outlined in ref. [23]. The data in fig. 4 shows that the echo can be observed which proves that the decay of the oscillation is not caused by incoherence. One can see that the features of the echo are symmetric around $\tau = 2\tau_{180} = 400$ns and, that they match qualitatively the features of the dephasing transient at the beginning of the pulse. From a fast Fourier transform (FFT) of the grey shaded time interval of the data in fig. 4 one can obtain a much better resolution of the frequency components contained in Q(t) in comparison to the interval between $\tau = 0$ and 200ns (this is not shown here since the FFT data is discussed in detail in the next paragraph).

The rotary echo experiment presented in fig.4 was repeated with a phase change time $\tau_{180} = 256$ns for various magnetic fields in a range where magnetic resonant changes were observed as shown in fig. 3. The results of these measurements are displayed by a colour plot in fig. 5(a). In fig. 5(b) the FFT of the time between the phase jump at $\tau = \tau_{180} = 256$ns and the echo at $\tau = 2\tau_{180} = 512$ns is displayed. Note that the FFT(Q) is displayed as a function of the magnetic field that is shown. This two dimensional colour plot confirms the data obtained for a single magnetic field corresponding to $g = 2.005$ as displayed in fig. 4 and shows three topologically distinct areas where signals can be observed: (i) The single peak resonance around $g = 2.008$, the average of the two bandtail state resonances which belong to the Rabi frequency $\Omega_1 = 66.1$ MHz. The second and most pronounced feature actually consists of two topologically separate areas which

is counted as one signal because of the mutually perfectly symmetric shape of these areas around $g = 2.008$. The signal actually vanishes at this centre Landé factor whereas its peaks are close to the Landé factors of the conduction and valance bandtail states at, $g = 2.004$ and $g = 2.012$, respectively. This structure occurs at a Rabi frequency of $\Omega_2 \approx 44.7$ MHz $\approx \Omega_1/\sqrt{2}$. The third and least pronounced structure belongs to Landé factor of dangling bonds at $g \approx 2.005$. It shows some contribution to $g \approx 2.004$ and exhibits the Rabi frequency of $\Omega_3 = 33.1$ MHz $\approx \Omega_1/2$. Note that in contrast to the other components, the signal is much more narrow and visible only around the dangling bonds resonance.

5. Discussion and conclusions of the experimental results

The experimental data on i-a-Si:H shows that the wide peak, observed in the past with cw ODMR, consists of at least three distinct recombination mechanisms. Since the nutation frequencies of the centres involved in the observed oscillation had ratios of $1:\sqrt{2}:2$, we conclude that the signals with nutation frequency Ω_1 are strongly coupled systems whereas those with Ω_3 are weakly coupled systems. We attribute the Landé factor of $g = 2.008$ for the Ω_1 pairs to strongly exchange coupled electrons and holes in adjacent conduction and valence bandtail states, respectively. This explanation excludes implicitly that the Ω_1 process could be due to weakly coupled pairs with narrow Larmor separation since no paramagnetic center with $g = 2.008$ is conceivable otherwise in i-a-Si:H. The resonances which cause a nutation with frequency Ω_2 and which are widely and symmetrically distributed on the magnetic field scale can be attributed to electrons and holes in adjacent conduction and valence band tail states, respectively, again. In contrast to the Ω_3 process, exchange coupling appears to be much smaller so that their peak shape seems to be mostly influenced by dipolar interaction. The maxima of these peaks are close to the expected Landé factors of conduction and valence bandtail states whereas the distribution stretches over more than 5mT in each direction. This behaviour is in accordance with the known structure of randomly oriented dipolar coupled spin pairs convoluted with a distribution of the coupling strength due to the distribution of pair distances as expected for a disordered semiconductor. At this time, no theoretical study has been conducted predicting the nutation frequencies of dipolar coupled spin pairs. However, from pulsed ESR literature it is expected that the Rabi-nutation frequency of dipolar coupled spin pair will be in the order $\sqrt{2}\gamma B_1$

[28]. Thus, assumed that Ω_3 represents the nutation frequency of completely weakly coupled pair systems, the observed Rabi oscillation Ω_2 is in accordance with dipolar coupling as well.

We interpret the qualitatively different coupling situation for pairs of bandtail states with nutation frequencies Ω_2 and Ω_3 by an exchange coupling threshold which is passed when the distance within a pair passes under a certain limit: A quantitative evaluation of the distance distribution of the dipolar coupled signals [7,16] reveals that there is a strong decline of signal intensity below ≈ 10Å, thus we interpret the strongly exchange coupled pairs to tightly coupled charge carriers in adjacent bandtail states. In spite of all the differences to the nature of mobile excitons in crystalline semiconductors, they can be referred to as immobile, localized excitonic states. From fig. 3 one can deduce that both, the excitonic and the non-excitonic tail-tail recombination channels produce an enchancement of the PL intensities which means an increase of the PL rate after the microwave pulse. Under the given measurement conditions (high generation rates, random intermediate pair generation), one can conclude from this that the observed processes are radiative. This is in contrast to the third, small signal with nutation frequency Ω_3. This process exhibits completely different dynamics, weak coupling between the recombining charge carrier pairs, and, since it is detected on a real-time scale as quenching which means a decrease of the PL rate after the microwave pulse, it appears to be non-radiative and thus, optically detectable only through observation of the quenching of competing radiative recombination channels. This observation is interpreted as the signature of dangling bond recombination of distant excess charge carrier pairs as it has been observed before by cw EDMR experiments [14].

6. Summary

A review of pODMR and pEDMR spectroscopy on semiconductors has been given where the different types of spin-dependent electronic processes in semiconductors were discussed and the measurement techniques and methodologies of the electrical and optical detection of coherent spin motion was outlined. The application of these measurement approaches was demonstrated for the example of pODMR on nominally intrinsic a-Si:H which showed how many disorder related, qualitatively different, yet with cw EDMR or ODMR spectroscopies indistinguishable recombination channels, can be mapped out by simultaneous deconvolution into Landé factors and their coupling regimes. For the a-Si:H example, this showed that most of the PL is generated

by recombination between conduction and valence bandtail states whereas there are two well distinguishable coupling regimes, those with strong exchange coupling which are referred to as localized excitons and those with small exchange coupling which are dominated by dipolar coupling within the spin pairs. In addition, a third qualitatively different recombination channel was found which involved recombination through deep dangling bond states.

References

[1] J. Brossel, S. Geschwind, and A. L. Schawlow, Phys. Rev. Lett., **3** (12), 548 (1959).
[2] R. Maxwell and A. Honig, Phys. Rev. Lett., **17** (4), 188 (1966).
[3] M. Stutzmann, M. S. Brandt, and M.W. Bayerl, J. Non–Cryst. Solids **266-269**, 1 (2000).
[4] B. C. Cavenett, Advance in Physics 30, 475 (1981).
[5] M. Xia, I. Martin, E. Yablonovitch, and H. W. Jiang, Nature (London) **430**, 435 (2004).
[6] J. Wrachtrup, C. von Borczyskowski, J. Bernard, M. Orrit, and R. Brown, Nature (London) **363**, 244 (1993).
[7] K. Lips, C. Boehme, T. Ehara, J. Optoel Adv. Mat., **7**, (1) 13 (2005)
[8] C. Boehme and K. Lips, in Charge Transport in Disordered Solids with Applications in Electronics, edited by S. Baranovski (John Wiley and Sons, Ltd., Chichester, England, 2006), Chap. 5, pp. 179–219.
[9] F. Jelezko, T. Gaebel, I. Popa, A. Gruber, and J. Wrachtrup, Phys. Rev. Lett. **92**, 076401 (2004).
[10] A. Schweiger and G. Jeschke, Principles of pulse electron paramagnetic resonance (Oxford University press, Oxford, 2001).
[11] D. D. Awschalom, D. Loss, N. Samarth (Editors), Semiconductor Spintronics and quantum computation, (Springer, New York, 2002).
[12] M. Wohlgenannt, C. Yang, and Z. V. Vardeny, Phys. Rev. B **66**, 241201 (2002).
[13] T. Eickelkamp, S. Roth, and M. Mehring, Mol. Phys. **95**, 967 (1998).
[14] K. Lips and W. Fuhs, J. Appl. Phys. **74**, 6, 3993 (1993).
[15] J.-M. Spaeth and H. Overhof, Point Defects in Semiconductors and Insulators, (Springer, Berlin, 2002).
[16] C. Boehme, F. Friedrich, T. Ehara and K. Lips, Thin Solid Films, **487**, 132– 136 (2005).
[17] W. Fuhs, P. Kanschat, and K. Lips, **18**, 3, 1792 (2000).
[18] C. Boehme and K. Lips, Phys. Stat. Sol. C 1, 1255 (2004).
[19] D. Kaplan, I. Solomon, and N. F. Mott, J. Phys. (Paris) – Lettres 39, L51 (1978).
[20] C. Böhme, Dynamics of spin-dependent charge carrier recombination, (Cuvillier, Göttingen, 2003).
[21] D. J. Gravesteijn and M. Glasbeek, Phys. Rev. B **19**, 5549 (1979).
[22] C. Boehme and K. Lips, Phys. Rev. Lett., **91** (24), 246603 (2003).
[23] C. Boehme and K. Lips, Phys. Rev. B **68**, 245105 (2003).
[24] V Rajevac, C. Boehme, C. Michel, A. Gliesche, K. Lips, S. D. Baranovski and P. Thomas, quanth-ph:0607030 (2006).
[25] Pierz, W. Fuhs, H. Mell, Phil. Mag. B **63**, 123 (1991).
[26] B. C. Cavenett, S. P. Depinna, I. G. Austin, T. M. Searle, Phil. Mag. B **48**, 169 (1983).
[27] A. V. Astashkin, A. Schweiger, Chem. Phys. Lett. **174**, 595 (1990).
[28] A. Weber, O. Schiemann, B. Bode, T.F. Prisner, J. Magnetic Resonance **157**, 277 (2002).

to be published in: ***Journal of Material Science: Materials in Electronics***

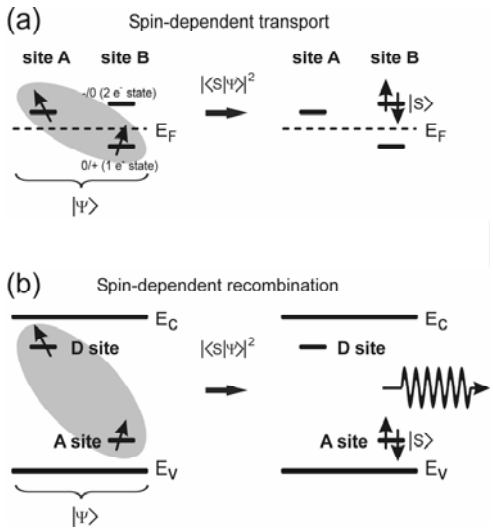

Fig. 1: Illustrations of the mechanism behind spin-dependent electronic transitions in semiconductors which are detectable with EDMR or ODMR: (a) Spin-dependent transport through localized states. Spin-dependent transition occur when two energetically different states A and B are in close proximity where the singly occupied (0/+) state of site A is energetically close to the doubly occupied (-/0) state of site B. (b) Spin-dependent recombination illustrated for the example of donor (D) – acceptor (A) recombination. Similar as for (a), spin-dependency requires a transition between two singly occupied paramagnetic states leading to one unoccupied and one doubly occupied, diamagnetic state.

to be published in: ***Journal of Material Science: Materials in Electronics***

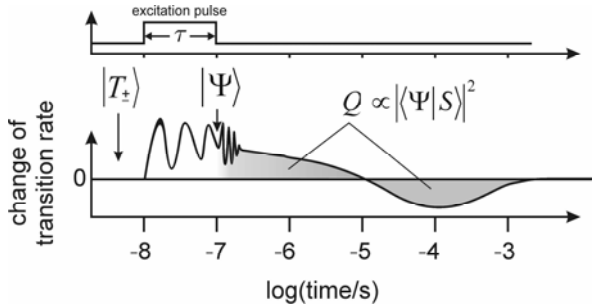

Fig. 2: Measurement of a coherent spin pair state by means of pulsed ODMR/EDMR illustrated on a logarithmic time scale: A system in a non-equlibrium steady state is excited by a short, intensive, coherent microwave pulse which increases the singlet content of the spin pairs and therefore an electronic transport or recombination rate. During the pulse the transition rate is governed by the Rabi oscillation of the excited electron spins. After the pulse, the rate slowly relaxes back to the steady state. The integral Q of this relaxation rate is a measurement of the permutation symmetry of spin pair states at the end of the pulse.

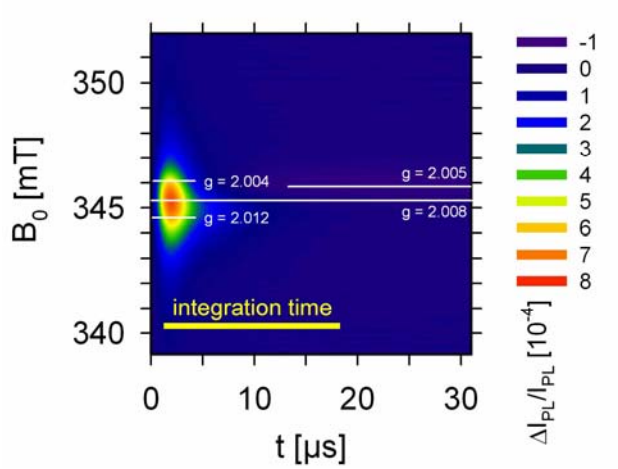

Fig. 3: Color plot of the transient of the relative PL change $\Delta I_{PL}/I_{PL}$ from the steady state of intrinsic a-Si:H as a function of different magnetic fields B_0 in the range between 339mT and 352mT after a short coherent microwave pulse with pulse length τ = 320ns is applied which ends at t = 0. The white lines indicate magnetic fields corresponding to the Landé factors of conduction band tail states ($g \approx 2.004$), valence band tail states ($g \approx 2.012$), dangling bonds ($g \approx 2.005$) as known from a-Si:H ESR spectroscopy [14] and $g \approx 2.008$, the average of the tail state Landé factors. The thick line displays the integration interval for the measurement of Q for the data sets displayed in figs. 4 and 5.

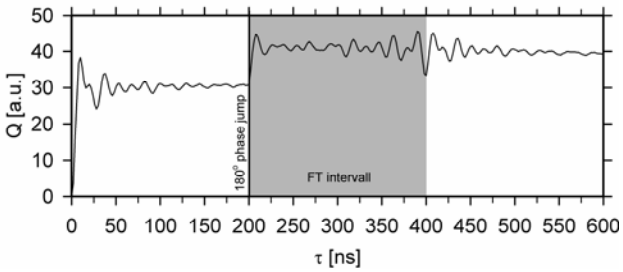

Fig. 4: Plot of Q as a function of the pulse length τ when the pulse undergoes a sudden phase change by 180° at τ_{180} = 200ns. The data was recorded at a magnetic field corresponding to g = 2.005. In the first 200ns of the pulse a decaying oscillation with various frequency components is measured. After the phase change, the dephased oscillation rephases and at maximum rephrasing, a so called recombination echo occurs at $\tau = 2\tau_{180}$ = 400ns. The grey area represents the pulse length interval where the data has to be transformed by a fast Fourier transform (FFT) in order to resolve the Rabi nutation components optimally.

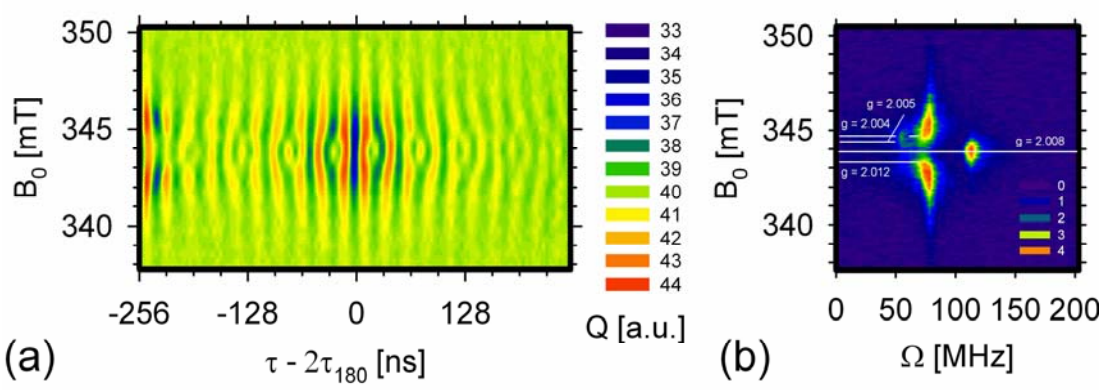

Fig. 5: (a) Colour plot of recombination echoes similar to the data presented for $g = 2.005$ in fig. 4. The plot represents Q measured as a function of the pulse length τ and the magnetic field B_0, for pulse lengths in the range of ±256ns around the echo which occurs at a $\tau = 2\tau_{180} = 512$ns. The experiment was conducted with a phase change time of $\tau_{180} = 256$ns. (b) The FFT(Q) for the data shown in (a) for the interval of $\tau - \tau_{180}$ between -256ns and 0. One can see distinct Rabi oscillation components at different magnetic fields. The white lines indicate magnetic fields corresponding to the Landé factors of conduction band tail states ($g \approx 2.004$), valence band tail states ($g \approx 2.012$), dangling bonds ($g \approx 2.005$) as known from a-Si:H ESR spectroscopy [14] and $g \approx 2.008$, the average of the tail state Landé factors.